Asian Journal of Civil Engineering (2023) 24:2669–2691
https://doi.org/10.1007/s42107-023-00623-3

ORIGINAL PAPER

A probabilistic approach for seismic demand estimation of steel moment frames considering capacity uncertainty

Behzad Shokrollahi Yancheshmeh[1] · **Mehdi Mahdavi Adeli**[2]

Received: 9 January 2022 / Accepted: 1 March 2023 / Published online: 4 May 2023

Abstract

Seismic demand estimation of steel moment-resisting frames (SMRF) is a function of uncertainties caused by using different ground motion records and capacity uncertainty due to the uncertainties of construction quality and model parameters that are usually obtained from a limited number of experimental data. To study the effect of capacity uncertainty, a set of SMRF was analyzed through incremental dynamic analysis (IDA) for two cases with and without such uncertainty. Latin hypercube sampling is used to consider the model's parameter uncertainty through the Monte Carlo simulation method. The fragility curves and the mean annual frequency (MAF) of the limit state for each case were extracted and the results have been compared. Moreover, the impact of construction quality on the estimation of MAF curves has been investigated. The results confirm the considerable effect of capacity uncertainty on increasing MAF at the collapse limit state.

Keywords Capacity uncertainty · Steel moment-resisting frame · Construction quality · Probabilistic seismic demand assessment · Collapse fragility · Mean annual frequency

Introduction

Probabilistic methods for seismic demand estimation of steel moment-resisting frames which include various uncertainties are one of the challenging issues of performance-based design in earthquake engineering. In a general classification, the sources of uncertainty can be divided into the inherent randomness (Aleatory uncertainty) caused using different earthquake records and the epistemic uncertainty owing to the model parameters or lack of knowledge. There are many studies on the uncertainties caused by the variable nature of different ground motion records. Capacity uncertainty is another factor affecting the seismic demand estimation of steel moment-resisting frames, which is due to doubts about the validity of the assumptions and information used for modeling. These may include but are not limited to the type of deterioration model applied, the degree of accuracy of the relationships presented to define the parameters of the deterioration model, construction quality, and lack of modeling knowledge. Therefore, a suitable estimation of demand and capacity quantities will be obtained if both types of uncertainty are applied. Hence, it is necessary to select the appropriate method to take into account capacity uncertainty and its impact on the probability of structural failure**.**

The investigation of the seismic hazard assessment method based on the fragility curves started by Shinozuka research (Shinozuka, 1998). He extracted the fragility curves for a bridge through a Monte Carlo simulation. Arizaga derived the fragility curves for 2, 3, 4, 6, 8, and 10-story steel moment-resisting frames using nonlinear dynamic analysis (Cortés-Areizaga, 2007). He developed fragility curves using FEMA regulations based on PGA as the intensity measure and inter-story drift ratio as the demand parameter (Agency, 2009). By performing the incremental dynamic analysis (IDA) and defining the failure criteria, the structural response can be determined (Vamvatsikos & Cornell, 2002). Kaveh et al. presented an ant colony optimization (ACO) method for the design of lightweight frame structures that fulfill multiple performance levels of seismic design constraints (Kaveh et al., 2010). They employed a computer-based method for the push-over analysis of steel

✉ Mehdi Mahdavi Adeli
mehmahad@yahoo.com

Behzad Shokrollahi Yancheshmeh
bshokrollahi@gmail.com

[1] Department of Civil Engineering, Institute for Higher Education ACECR, Khuzestan, Iran

[2] Department of Civil Engineering, Shoushtar Branch, Islamic Azad University, Shoushtar, Iran

building frameworks subjected to equivalent static earthquake loads. A design optimization procedure was developed for steel moment frames in high seismic zones, where member sectional sizes were almost exclusively determined by drift requirements. To illustrate the capabilities of the ACO procedure, two examples were considered. It was shown that ACO has the advantage of being less affected by poor initial solutions when compared to traditional genetic algorithms (GAs). Moreover, it is more successful than GA at predicting the optimum seismic design of structures. In recent years, some research has been conducted to evaluate the effect of epistemic capacity uncertainty on the structural response using a 9-story steel moment-resisting frame with capacity uncertainty as the case study (Ibarra & Krawinkler, 2011; Vamvatsikos, 2014; Vamvatsikos & Fragiadakis, 2010). Based on the sensitivity analysis of the system response due to changes in moment-rotation relationships of plastic hinges located at the end of beams, they concluded that capacity uncertainty has an important role in increasing dispersion in performance estimation. Furthermore, the idea that the base model (mean parameter) results in the median seismic capacity and demand has been rejected, but the base model can still be acceptable for practical applications. Ibarra and Krawinkler showed that in deteriorating hysteresis models, uncertainties due to model parameters would have a significant impact on the estimation of structural performance in a collapse state (Ibarra & Krawinkler, 2011). However, this study was limited to one-degree-of-freedom systems, and validation for the extension to multi-degree-of-freedom models has not been specified. Vamvatsikos studied the seismic performance of a 9-story steel moment frame to consider capacity uncertainty using progressive ground motion record-wise through Lain hypercube sampling (Vamvatsikos, 2014). The aforementioned method is an effective algorithm for estimating model parameter uncertainties by random sampling but with fewer samples than the previous methods. In this method, instead of applying the changes of any model parameter to all earthquake records, each record has a model with different parameters than other records. He found that the convergence rate of the model is high in comparison with the previous methods and the capacity uncertainty can be evaluated with less sampling. Kaveh et al. used A Non-dominated Sorting Genetic Algorithm (NSGA-II) as the optimization algorithm enhanced by applying a Differential Evolution operator (DE) and a polynomial mutation operator to search for Pareto optimal solutions (Kaveh et al., 2015). They proposed a framework for the performance-based multi-objective optimal design of steel moment-frame structures through nonlinear dynamic analysis. To reduce the number of acceleration points involved, a wavelet decomposition process was applied. The time history response of structures was predicted using a fitness approximation strategy. Results indicated that the program was capable of reducing computational effort by a significant amount. A comparison was conducted between nonlinear static analysis (NSA) and nonlinear time history analysis (NTHA) for scaled earthquakes in order to assess the response of semi-rigid frames (with different degrees of semi-rigidity) to three different types of earthquakes (Sharma et al., 2020). Two frames with different heights (5-story and 10-story frames) were considered. Responses were compared in terms of root mean square errors (Erms). It was shown that the nonlinear static analysis provided a fairly reliable estimate of the peak values of top story displacements and peak base shear for all cases. Additionally, for the five-story frame, the NSA method produced reasonable predictions of the maximum inter-story drift, whereas for the ten-story frame, the results were extremely poor. In addition, the NTHA provided a greater number of plastic hinges for rigid frames than the NSA, but the number of plastic hinges formed in semi-rigid frames was reduced in both methods. A comparative study was carried out by Sharma et al. to estimate seismic energy losses between semi-rigid steel frames modeled in two different approaches and rigid steel frames under near-field and far-field earthquakes with forward directivity and fling step effect (Sharma et al., 2021). To evaluate the desired responses, a nonlinear response history analysis was conducted using SAP2000 software for two peak ground acceleration levels for three variants of earthquakes. Results indicated that rigid and semi-rigid frames dissipate seismic energy differently. Among semi-rigid frames, modal energy consumes the majority of the seismic energy, whereas link hysteretic energy consumes a much smaller proportion. As compared to rigid frames, semi-rigid frames exhibit the greatest roof displacement values and the least amount of base shear. Furthermore, semi-rigid frames with multi-linear plastic links performed significantly better during earthquakes than rigid frames or semi-rigid frames with multi-linear elastic links. A 10-story semi-rigid steel frame subject to near- and far-field earthquakes was evaluated using fragility analysis by taking into account a variety of damage measures (Sharma et al., 2021). In addition, the effects of frequency contents on structural damages as measured by the PGA to PGV ratio were examined. It was shown that the fragility curves for the maximum inter-story drift ratio (MIDR) and maximum roof drift angle (Ψ max) were more sensitive to the type of earthquakes. Moreover, the probability of exceedance (POE) for all damage measures except the Ψ max was high for the slight damage state. A high POE for extensive and complete damage states was observed for all damage measures in near-field earthquakes with a high directivity effect. As a result of the study, it was concluded that the PGV to PGA ratio of a near-field earthquake with a directivity effect had an influential impact on the POE of different damage states. Segura Jr. et al. developed a methodology to quantify uncertainty in

the mechanical properties of reinforcing steel and concrete as well as their impact on the seismic response of reinforced concrete bridge columns (Segura et al., 2022). A statistical distribution of key material properties for steel and concrete with specific compressive strengths was implemented for performance-based seismic evaluations. Dispersion in the column force demand and maximum absolute drift ratio were employed to quantify seismic response uncertainty. An analytical model has been developed and tested on the shaking table to evaluate the impact of material uncertainty on seismic performance evaluations. The endurance time analysis (ETA) method was used to conduct nonlinear analyses in OpenSees. The authors found that the analytical results were most sensitive to material properties that define the hardening branch of the concrete stress–strain curve and the elastic branch of the reinforcing steel stress–strain curve. Moreover, the uncertainty in the column deformation response was higher for model combinations with a higher specified steel strength and a lower specified concrete strength.

Knowing that the fragility curves give the collapse probability of structures due to the selected earthquake records for a given limit state, it is not possible to investigate the occurrence probability of earthquakes in these curves. Therefore, to comprehensively investigate the probabilistic estimation of seismic demand for steel moment frames, the mean annual frequency of collapse should be calculated. The mean annual frequency of collapse, λ_c, is estimated through the calculated collapse fragility curve combined with the seismic ground motion hazard curve of the site. Previous studies have not focused enough on the impact of capacity uncertainty on λ_c estimation. Therefore, it is necessary to study the effect of this epistemic uncertainty on calculating the mean annual frequency of the collapse limit state. Procedures for probabilistic seismic assessment start with the selection of an acceptable number of earthquake records including an appropriate range of desired specifications such as magnitude, focal length from the fault center, and site conditions. The next step is to select an appropriate intensity measure, which is usually considered to be maximum ground motion acceleration, PGA, or the Spectral acceleration of fundamental mode with damping, S_a (T_1, ξ). Structural behavior is expressed by defining mechanical properties and deterioration model parameters.

In the present study, 7 steel moment-resisting frames are investigated. The modified Ibarra–Medina–Krawinkler (IMK) deterioration model was used to reflect the nonlinear behavior of the structure (Ibarra et al., 2005). Considering that the model parameters were obtained based on a limited number of laboratory samples, the application of these quantities is associated with uncertainty. The model's parameter uncertainty has been applied through progressive ground motion record-wise Latin hypercube sampling (Vamvatsikos, 2014). IDA for a set of 80 ground motion records was performed for two models: the base model that only incorporates the uncertainty due to using various ground motion records and the uncertain model that considers both aleatory and epistemic uncertainties. Fragility curves were derived for both models. The aforementioned uncertainty caused the mean and standard deviation of the uncertain model to differ from the base model. Furthermore, the validity of the classic notion of using the base model median for the uncertain model and its effect on λ_c estimation has been reviewed and investigated. Additionally, to investigate the dependency of λ_c on the statistical parameters of the fragility function, a sensitivity analysis of the results is performed for a 20-story frame based on independent variations of statistical parameters from the uncertain model in comparison with the base model. Moreover, construction quality is considered another source of capacity uncertainty and λ_c of the base and uncertain models (including both the model's parameter and the construction quality uncertainties) are calculated and compared.

Steel frames description

The steel moment-resisting frame building in the city of Century, California is intended for consideration (Mathiasson & Medina, 2014). The 20-story building was designed according to load and resistance factor design specifications (LRFD) based on ASCE provisions (Committee, 2010). The building plan is shown in Fig. 1. The lateral load-resisting system in both directions comprises a pair of steel moment-resisting frames that are very common in seismic-prone areas. In this study, one of the N–S perimeter frames is selected. W-sections with 350 MPa yield stress and 200 GPa modulus of elasticity were considered (Appendix) (Mathiasson & Medina, 2014). Due to the type of lateral load-resisting system, a pinned leaning column was added to the frame to simulate the P-Δ effect caused by the interior gravity load-resisting frames. The concentrated plasticity approach is considered to define the nonlinear behavior of the structure. Accordingly, the beams and columns are considered elastic elements, and non-linear rotational springs are placed at the ends of the beams. The nonlinear behavior of the springs is defined by the modified Ibarra–Medina–Krawinkler (IMK) deterioration model with a bilinear hysteretic response as depicted in Fig. 2 (Ibarra et al., 2005). Lignos and Krawinkler derived the parameters of the model based on the results of more than 300 specimens that are used to improve the IMK model (Lignos & Krawinkler, 2011). They also used statistical methods with this data set to develop empirical equations to predict model parameters. To comprehensively investigate the effect of capacity uncertainty, 6 more frames including 3, 5, 7, 9, 12, and 15-story frames (having similar building plans to the 20-story frame) are also designed and

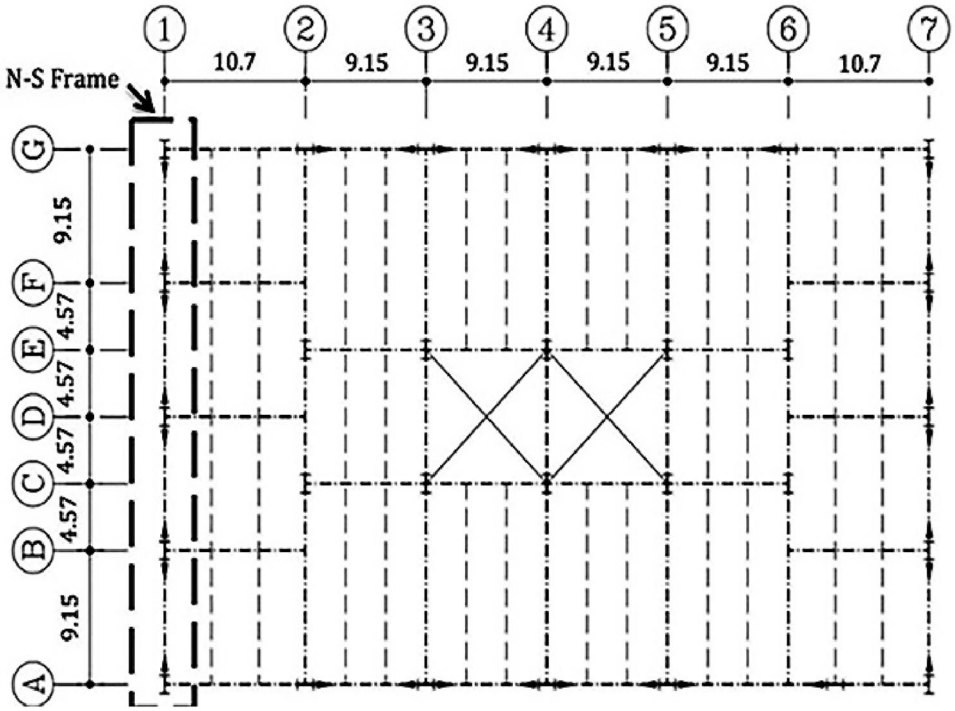

Fig. 1 Typical floor plan (Mathiasson & Medina, 2014)

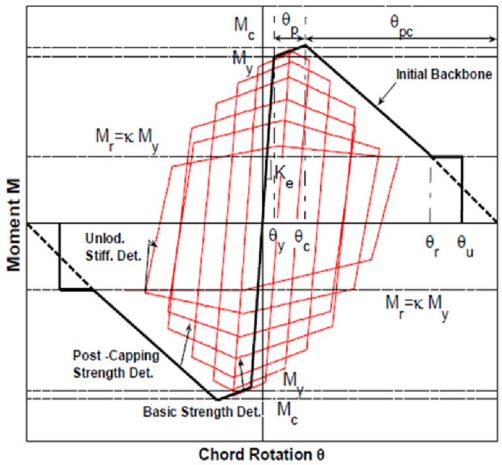

- Effective yield strength and rotation (M_y and θ_y)
- Effective stiffness K_e=M_y/θ_y
- Capping strength and associated rotation for monotonic loading (M_c and θ_c)
- Pre-capping rotation capacity for monotonic loading θ_p
- Post-capping rotation capacity θ_{pc}
- Residual strength $M_r = \kappa M_y$
- Ultimate rotation capacity θ_u

Fig. 2 Deterioration model (Ibarra et al., 2005)

studied (Appendix). The height of the first story is 4.57 m and the rest of the stories are 3.96 m.

Gravity loads are determined according to the load combinations of FEMA P695 which is 1.05D + 0.25L where D is the dead load and L is the live load (Agency, 2009). To use suitable seismic hazard curves, the eigenvalue analysis for the frame was performed by OpenSees software (McKenna, 2011). Periods for the first mode of vibration of all 7 frames are shown in Table 1.

Table 1 The first mode vibration period of the considered steel frames

No. of stories	T_{sec}
3	0.58
5	0.99
7	1.38
9	1.66
12	2.06
15	2.4
20	2.84

Earthquake records selection

The ground motion records were selected according to the magnitudes and the nearest distance to fault rupture. In other words, some intervals for the above-mentioned parameters are defined, and records are selected according to the characteristics of these intervals. The definition of these intervals should be such that they first include destructive earthquakes, and second, they would be likely to occur within the specified target range. In this study, the magnitude of an earthquake between 5.8 and 7.0 Richter was selected and divided into two intervals of (5.8 to 6.5) and (6.5 to 7.0).

The magnitude of an earthquake below 5.8 Richter is not so destructive, and more than 7.0 Richter is less probable to occur. Besides, it is very difficult to find a corrected and standardized record with a magnitude greater than the above values. In addition, the range for the closest distance to fault rupture defined in the present study is between 13 and 60 km which is divided into two intervals of (13 to 30) and (30 to 60) km. An earthquake with the nearest distance to fault rupture less than 13 km is often defined as a near-field earthquake and it contains uncertainties that are not considered in the present study. On the other hand, earthquakes with a distance of more than 60 km far from structures are less destructive. According to the above descriptions, four sets of ground motions are considered as follows:

- Large magnitude ($6.5 < MW < 7.0$) and short-distance ($13\ km < R < 30\ km$), referred to as LMSR.
- Large magnitude ($6.5 < MW < 7.0$) and long-distance ($30\ km < R < 60\ km$), referred to as LMLR.
- Low magnitude ($5.8 < MW < 6.5$) and short-distance ($13\ km < R < 30\ km$), referred to as SMSR.
- Low magnitude ($5.8 < MW < 6.5$) and long-distance ($30\ km < R < 60\ km$), referred to as SMLR.

To complete the selection process, an appropriate number of ground motion records should be selected for each set. To increase the reliability of the results, a large number of records with different frequency contents, i.e. 80 ground motions (20 records for each set), were selected for nonlinear dynamic analysis. Records were selected from the Pacific Earthquake Engineering Research Center PEER ground motion database (Center, 2013; Medina & Krawinkler, 2004). None of the selected records are near-fault records and hence do not have near-field effects. The site classification of these records is according to the NEHRP Class D classification (Council, 2009). None of these records are after-shock or pre-aftershock, and all of them are due to the main shock. To prevent a particular earthquake from affecting the results, each record is randomly selected among the two horizontal components of a station. The specific characteristics of the selected records are given in Tables 2, 3.

Incremental dynamic analysis (IDA)

Base model

The IDA is performed on a set of 80 selected ground motion records based on the model parameters defined in the base model. The intensity measure (IM) and engineering demand parameter (EDP) should be carefully selected to ensure a reliable interpretation of IDA results. Intensity measures commonly used (but not limited to) are peak ground acceleration (PGA), peak ground displacement (PGD), and fundamental mode spectral acceleration Sa(T1, 5%). Some demand parameters that have been considered in previous studies include roof displacement, peak story displacement, seismic energy, plastic hinges, and maximum interstory drift ratio. According to Shome and Cornell (1999), IDA curves derived based on Sa(T1, 5%) intensity measure are less scattered than those derived from PGA intensity measure (Shome, 1999).

In the present study, PGA and the fundamental mode spectral acceleration with a 5% damping ratio Sa(T1, 5%) were selected as candidates for intensity measures since seismic hazard curves are readily available for both. Based on a linear regression model on a logarithmic scale, the relationship between the intensity measure and the median demand parameter can be considered as a straight line (Fig. 3) (Jalayer & Cornell, 2004). The results indicated that dispersion from the median line using Sa(T1, 5%) as an IM is less than dispersion associated with the PGA intensity measure except for the 20-story frame which is in reasonable agreement with the previous studies (Table 4). It was concluded that, although Sa(T1, 5%) is not necessarily the most suitable IM, especially for high-rise buildings (Adeli et al., 2012), it was chosen in this study to compare results for different story frames.

The maximum inter-story drift ratio (a displacement-based parameter) is considered to be a demand parameter. In accordance with FEMA350, for moment-resisting frames, it is an acceptable measure of global collapse (Hamburger et al., 2000). Furthermore, it can represent the nonlinear behavior of plastic hinges located at the ends of beams and columns.

The global collapse criterion is considered to exceed the 10% maximum inter-story drift ratio (Hamburger et al., 2000; Medina & Krawinkler, 2004). Each record is analyzed with 0.05 g increments of IM at each step until the model reaches the defined collapse criterion. The results of the IDA analysis for 7 frames are shown in Figs. 4, 5.

Uncertain model

In the present study, the uncertainty considered is due to the model parameters and the quality of construction. Accordingly, the mentioned uncertainty is expressed in the form of the following equation:

$$\left(\beta_u = \sqrt{\beta_m^2 + \beta_c^2}\right) \tag{1}$$

where β_m is due to model parameters and β_c is related to construction quality.

To introduce model parameter uncertainty, the uncertainties of the modified Ibarra–Medina–Krawinkler deterioration model are applied by perturbing backbone

Table 2 LMSR and LMLR suite of ground motion records (Center, 2013)

LMSR						LMLR					
Event	Year	M_W	Station	R (km)	PGA (g)	Event	Year	M_W	Station	R (km)	PGA (g)
Loma Prieta	1989	6.9	Agnews State Hospital	28.2	0.172	Borre Mountain	1968	6.8	El Centro Array #9	46.0	0.057
Loma Prieta	1989	6.9	Capitola	14.5	0.443	Loma Prieta	1989	6.9	AP.2E Hayward Muir	57.4	0.171
Loma Prieta	1989	6.9	Gilroy Array #3	14.4	0.367	Loma Prieta	1989	6.9	Fremont-Emerson Co	43.4	0.141
Loma Prieta	1989	6.9	Gilroy Array #4	16.1	0.212	Loma Prieta	1989	6.9	Halls Valley	31.6	0.134
Loma Prieta	1989	6.9	Gilroy Array #7	24.2	0.226	Loma Prieta	1989	6.9	Salinas-John & Work	32.6	0.112
Loma Prieta	1989	6.9	Hollister City Hall	28.2	0.247	Loma Prieta	1989	6.9	Palo Alto-SLAC Lab	36.3	0.194
Loma Prieta	1989	6.9	Hollister Diff Array	25.8	0.279	Northridge	1994	6.7	Covina-W Badillo	56.1	0.100
Loma Prieta	1989	6.9	Sunnyvale-Colton Av	28.8	0.207	Northridge	1994	6.7	Com.-Castlegate St	49.6	0.136
Northridge	1994	6.7	Canoga Park-Topanga	15.8	0.420	Northridge	1994	6.7	LA-Centinela St	30.9	0.322
Northridge	1994	6.7	LA–N Faring Rd	23.9	0.273	Northridge	1994	6.7	Lakewood-Del Am	59.3	0.137
Northridge	1994	6.7	LA-Fletcher Dr	29.5	0.240	Northridge	1994	6.7	Downey-Co.Maint	47.6	0.158
Northridge	1994	6.7	Glendale-Las Palmas	25.4	0.206	Northridge	1994	6.7	Bell Gardens-Jabo	46.6	0.068
Northridge	1994	6.7	LA-Hollywood StorFF	25.5	0.231	Northridge	1994	6.7	Lake Hughes #1	36.3	0.087
Northridge	1994	6.7	LaCrescenta-NewYork	22.3	0.159	Northridge	1994	6.7	Lawndale-Osage Ave	42.4	0.152
Northridge	1994	6.7	Northridge-Saticoy St	13.3	0.368	Northridge	1994	6.7	Leona Valley #2	37.7	0.063
San Fernando	1971	6.6	LA-Hollywood Lot	21.2	0.174	Northridge	1994	6.7	Palmdale-Hwy 14	43.6	0.067
Superstition Hill	1987	6.7	Brawley	18.2	0.156	Northridge	1994	6.7	LA-Pico & Sentous	32.7	0.186
Superstition Hill	1987	6.7	El Centro Imp.Cent	13.9	0.358	Northridge	1994	6.7	West Covina-S.Orange	54.1	0.063
Superstition Hill	1987	6.7	Plaster City	21.0	0.186	Northridge	1994	6.7	TerminalIsland-S	60.0	0.194
Superstition Hill	1987	6.7	Westmorland Fire St	13.3	0.172	Northridge	1994	6.7	LA-Evernon Ave	39.3	0.153

parameters around its mean (i.e., the base-case values). In the present study, model parameters vary as random variables within the range defined as follows:

$$(\mu - \sigma, \mu + \sigma) \tag{2}$$

where σ denotes the standard deviation and μ is the mean of each parameter (i.e. the base model value). The parameters considered to apply the uncertainties include M_y, θ_p, θ_{pc}, $\theta_{u,}$ Λ where Λ is the cyclic deterioration parameter (Lignos & Krawinkler, 2012). Accordingly, the maximum capacity of energy dissipation can be expressed as follows:

$$E_t = \lambda.\theta_P.M_y = \wedge.M_y \tag{3}$$

where $\Lambda = \lambda \cdot \theta_p \cdot M_y$ denotes maximum rotation capacity and M_y and θ_p represent effective yield moment and pre-capping plastic rotation, respectively.

The coefficient of variation considered for each parameter is given in Table 5. The values assigned to each parameter are taken into account based on previous studies

Table 3 SMSR and SMLR suite of ground motion records (Center, 2013)

SMSR						SMIR					
Event	Year	M_W	Station	R (km)	PGA (g)	Event	Year	M_W	Station	R (km)	PGA (g)
Imperial Valley	1979	6.5	Calipatria Fire Station	23.8	0.078	Borrego	1942	6.5	El Centro Array #9	49.0	0.068
Imperial Valley	1979	6.5	Chihuahua	28.7	0.270	Coalinga	1983	6.4	Parkfield-Cholame 5	47.3	0.131
Imperial Valley	1979	6.5	El Centro Array #1	15.5	0.139	Coalinga	1983	6.4	Parkfield-Cholame 8	50.7	0.098
Imperial Valley	1979	6.5	El Centro Array #12	18.2	0.116	Imperial Valley	1979	6.5	Coachella Canal #4	49.3	0.128
Imperial Valley	1979	6.5	El Centro Array #13	21.9	0.139	Imperial Valley	1979	6.5	Compuertas	32.6	0.186
Imperial Valley	1979	6.5	Cucapah	23.6	0.309	Imperial Valley	1979	6.5	Delta	43.6	0.238
Imperial Valley	1979	6.5	Westmor. Fire Station	15.1	0.110	Imperial Valley	1979	6.5	Niland Fire Station	35.9	0.109
Livermore	1980	5.8	San Ram.-East Kodak	17.6	0.076	Imperial Valley	1979	6.5	Plaster City	31.7	0.057
Livermore	1980	5.8	San Ram. Fire Station	21.7	0.040	Imperial Valley	1979	6.5	Victoria	54.1	0.167
Morgan Hill	1984	6.2	Agnews State Hospital	29.4	0.032	Livermore	1980	5.8	Tracy-Sewage Treat	37.3	0.073
Morgan Hill	1984	6.2	Gilroy Array #2	15.1	0.162	Morgan Hill	1984	6.2	Capitola	38.1	0.099
Morgan Hill	1984	6.2	Gilroy Array #3	14.6	0.194	Morgan Hill	1984	6.2	Hollister City Hall	32.5	0.071
Morgan Hill	1984	6.2	Gilroy Array #7	14.0	0.113	Morgan Hill	1984	6.2	San Juan Bautista	30.3	0.036
Point Mugu	1973	5.8	Port Hueneme	25.0	0.112	N. Palm Springs	1986	6.0	San Jacinto Valley C	39.6	0.063
N. Palm Springs	1986	6.0	Palm Springs Airport	16.6	0.187	N. Palm Springs	1986	6.0	Indio	39.6	0.064
Whittier Narrow	1987	6.0	Com.-Castlegate St	16.9	0.332	Whittier Narrow	1987	6.0	Downey-Birchdale	56.8	0.299
Whittier Narrow	1987	6.0	Carson-Catskill Ave	28.1	0.042	Whittier Narrow	1987	6.0	LA-Century City CC	31.3	0.051
Whittier Narrow	1987	6.0	Brea-S Flower Ave	17.9	0.115	Whittier Narrow	1987	6.0	LB-Harbor Admin FF	34.2	0.071
Whittier Narrow	1987	6.0	LA-W70thSt	16.3	0.151	Whittier Narrow	1987	6.0	Terminal Island-S	35.7	0.042
Whittier Narrow	1987	6.0	Carson-Water St	24.5	0.104	Whittier Narrow	1987	6.0	Northridge-Saticoy St	39.8	0.118

(Vamvatsikos & Fragiadakis, 2010). The reason for choosing less value to M_y is its severe impact on results. Generation of random variables is done by selecting 80 random (normally distributed) numbers with equal probability of occurrence in the interval $(\mu - \sigma, \mu + \sigma)$.

The uncertainties due to the construction quality are considered under the criteria of FEMA P-58-1 in the form of adding standard deviation based on the quality of construction in the three categories of superior, average, and limited quality as given in Table 6. (Fema, 2012). Accordingly, IDA analysis and extraction of fragility curves are performed based on the application of model parameter uncertainty and in the next step, uncertainty due to the construction quality is added to the standard deviation obtained from the analysis. The results of IDA analysis for uncertain models (including model parameter uncertainty) are shown in Figs. 6, 7.

Fragility curves

The fragility of a structure for a given limit state is the exceeding probability of the limit state's capacity for a specified Intensity Measure (IM), which is called a conditional

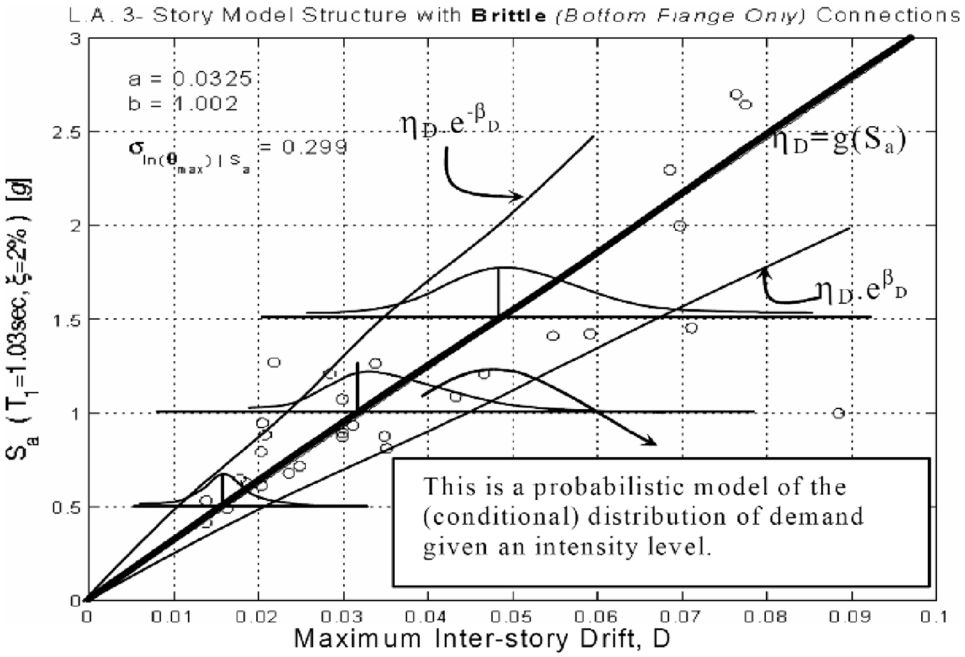

Fig. 3 Regression model for median demand parameter (Jalayer & Cornell, 2004)

Table 4 Dispersion from the median line (all frames)

Story No	Dispersion	
	PGA	S_a (T_1, 5%)
3	0.362	0.298
5	0.422	0.331
7	0.425	0.343
9	0.422	0.379
12	0.509	0.417
15	0.449	0.431
20	0.448	0.471

probability of collapse. If the intensity measure is expressed based on the spectral acceleration, the fragility can be defined as follows (Jalayer & Cornell, 2004).

$$F_{LS}(S_a) = p[S_a \geq S_{a,C} | S_a = s_a] = p[S_{a,c} \leq s_a] \quad (4)$$

where $F_{Ls}(S_a)$ is the fragility of the structure at the intensity measure (i.e. spectral acceleration) S_a for a given limit state. By inspecting the above formula, it is seen that fragility can be expressed as the probability of a random variable $S_{a,c}$ which is less than or equal to the given value S_a. In other words, fragility is a cumulative distribution function (CDF) of the capacity random variable. If the probabilistic distribution of the capacity spectral acceleration is considered as lognormal with a median μ and a standard deviation σ, the fragility will be as follows:

$$F_{LS}(S_a) = p[S_{a,C} \leq s_a] = \phi\left(ln\left(\frac{s_a}{\mu_{S_a,C}} \right) \right) / \beta_{S_a,C}) \quad (5)$$

According to the above equation, for each limit state, the fragility curve can be depicted as a function of intensity measure. The curve shape will always be an ascending function.

The fragility curves of the base model simply contain the inherent uncertainty resulting from earthquake records. In contrast, the fragility curve of the uncertain model also includes the uncertainty caused by the model parameters. Accordingly, the fragility curves using the results of IDA analysis for the immediate occupancy (IO) limit state (2% maximum inter-story drift ratio) and collapse prevention (CP) limit state (10% maximum inter-story drift ratio) using lognormal statistical distribution have been prepared and drawn for all the studied frames (Figs. 8, 9) (Hamburger et al., 2000). In addition, the mean μ and standard deviation σ of fragility curves are presented in Table 7. To better interpret the obtained results, the variation of the dimensionless parameters of the median ratio (μ_b/μ_u) and standard deviation (σ_u/σ_b) as functions of the demand parameter has been calculated. The results are displayed in Figs. 10, 11.

It is clearly shown in Figs. 10, 11 that there is no significant difference between the median and standard deviation of the uncertain model compared to the base model in the demand parameter range of less than 3%. Since in relatively small demand parameter values (less than 2%) the behavior of the structure according to the modified Ibarra-Medina-Krawinkler deterioration model (Fig. 2) is

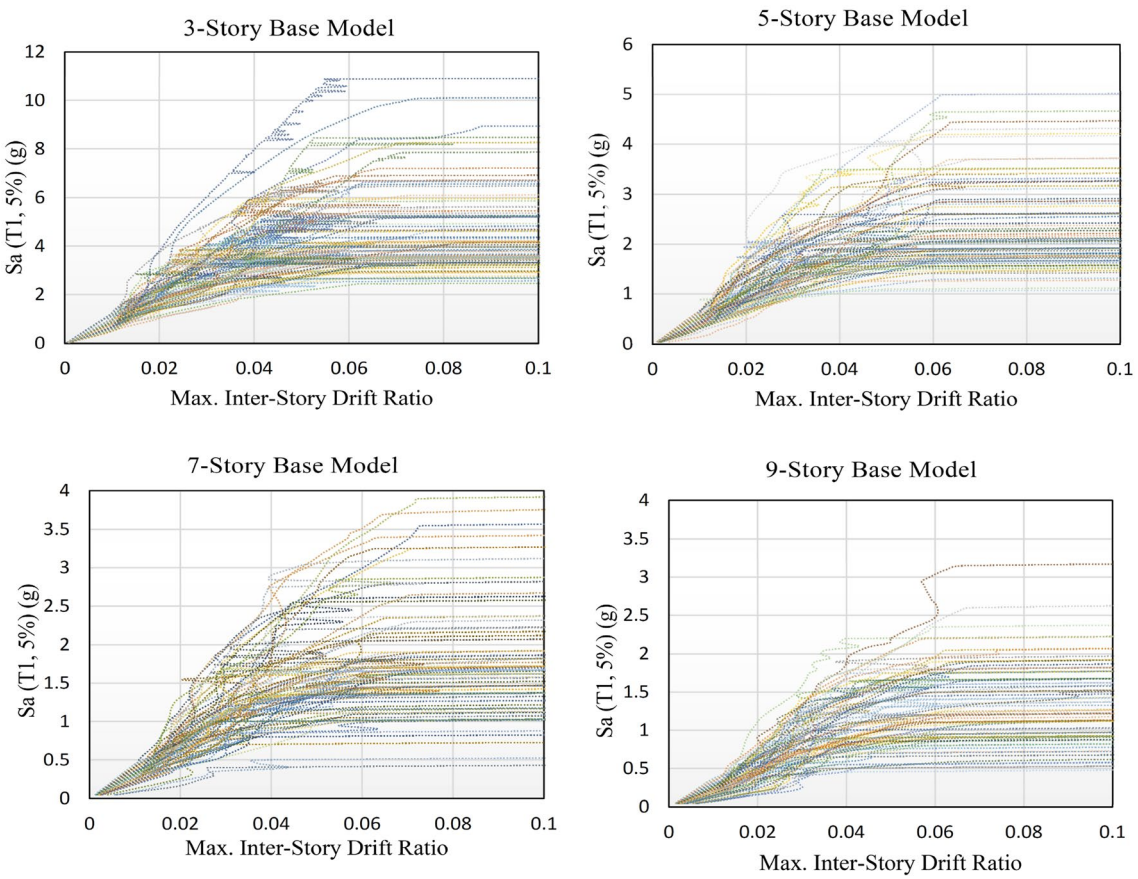

Fig. 4 IDA curves for 3–9 story frames (base models)

relatively linear, therefore only the M_y and θ_p parameters of the model (which change in the form of random variables in the specified interval) affect the behavior of the uncertain model, and the rest of the parameters do not affect the response of the structure. On the other hand, in the range of large demand parameters (more than 3%), all parameters of the model are involved in the response of the structure, and also due to the high relative displacement of the stories, the second-order effects of P-Δ are another factor to intensify the response. To apply the uncertainty due to the quality of construction (according to Table 6), the parameters of the fragility curves for the uncertain models are recalculated taking into account the construction quality and the results for the average construction quality are given in Table 8. It should be noted that fragility curves only indicate the probability of exceeding a certain limit state for a specified intensity measure, and the probability of earthquakes that cause this level of intensity measure is not considered. Therefore, to evaluate the effect of capacity uncertainty on the seismic demand assessment of steel moment frames, the calculation of the mean annual frequency for each limit state seems to be necessary.

Using the fragility curves in combination with the seismic hazard curve, the mean annual frequency at the IO and CP limit states for the base and the uncertain models can be calculated and compared, which has been studied in the following sections.

Seismic hazard curve

The hazard corresponding to a given IM denoted by $H_{\mathrm{Sa}}(x)$ is defined and represented by the average annual frequency that the future ground motion records' intensity is equal to or greater than that specific value x. It can be defined as the product of the number of occurring earthquakes (ν) by the probability of exceeding an IM (i.e. spectral acceleration) of a given value x, denoted by $G_{\mathrm{Sa}}(x)$ as follows (Jalayer & Cornell, 2004):

$$H_{S_a}(x) = \nu . G_{S_a}(x) \tag{6}$$

If the seismic hazard curve versus the spectral acceleration $S_{\mathrm{a\ is}}$ plotted, the seismic hazard diagram will be obtained. These curves are usually extracted by

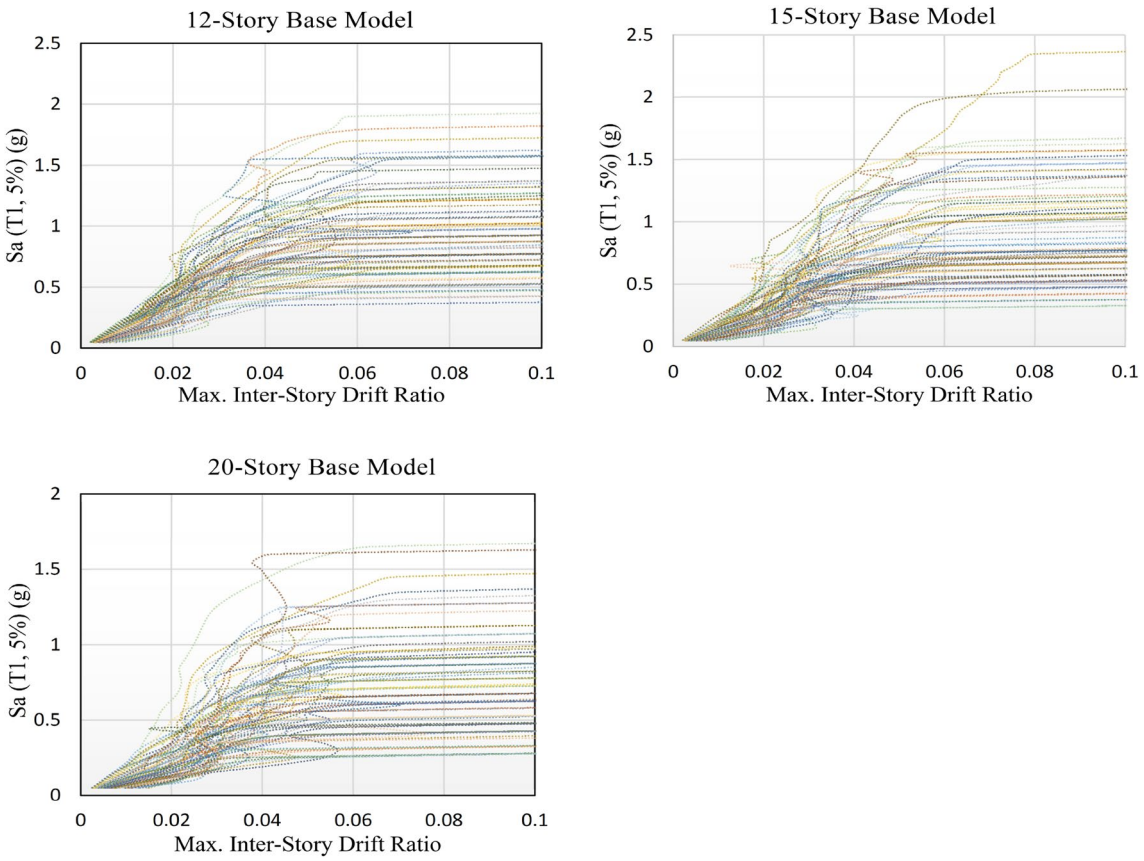

Fig. 5 IDA curves for 12–20 story frames (base models)

Table 5 Coefficient of variation of model parameters

Parameter	M_y	θ_p	θ_{pc}	θ_u	Λ
σ/μ	0.2	0.4	0.4	0.4	0.4

Table 6 Construction quality dispersion values (Fema, 2012)

Construction quality	β_c
Superior quality	0.10
Average quality	0.25
Limited quality	0.40

seismologists for a given site. Each curve contains the mean annual frequency of passing a specific value of IM for a given vibration period and damping ratio. If the curve in the desired range is approximated through a power law, the following equation will be obtained (Luco & Cornell, 1998):

$$H_{S_a}(S_a) = P[S_a \geq x] = k_0.x^{-k} \tag{7}$$

where the coefficients k_0 and k define the shape of the hazard curve. In the present study, the seismic hazard curves of Century City are investigated.

The seismic hazard curve for the Century with a period range of 0.5–3 s and a 5% damping ratio is shown in Fig. 12 (Center, 2013).

Mean annual frequency (MAF)

MAF is defined as the mean annual frequency of exceeding a specific limit state denoted by λ_{LS} which can be given for continuous functions as follows (Jalayer & Cornell, 2004):

$$\begin{aligned}\lambda_{LS} &= \nu.P[S_a \geq S_{a,C}] \\ &= \int P[S_a \geq S_{a,C}|S_a = x]\nu.f_{S_a}(x).\,\mathrm{d}x \\ &= \int P[x \geq S_{a,C}].\left|\mathrm{d}H_{S_a}(x)\right|\end{aligned} \tag{8}$$

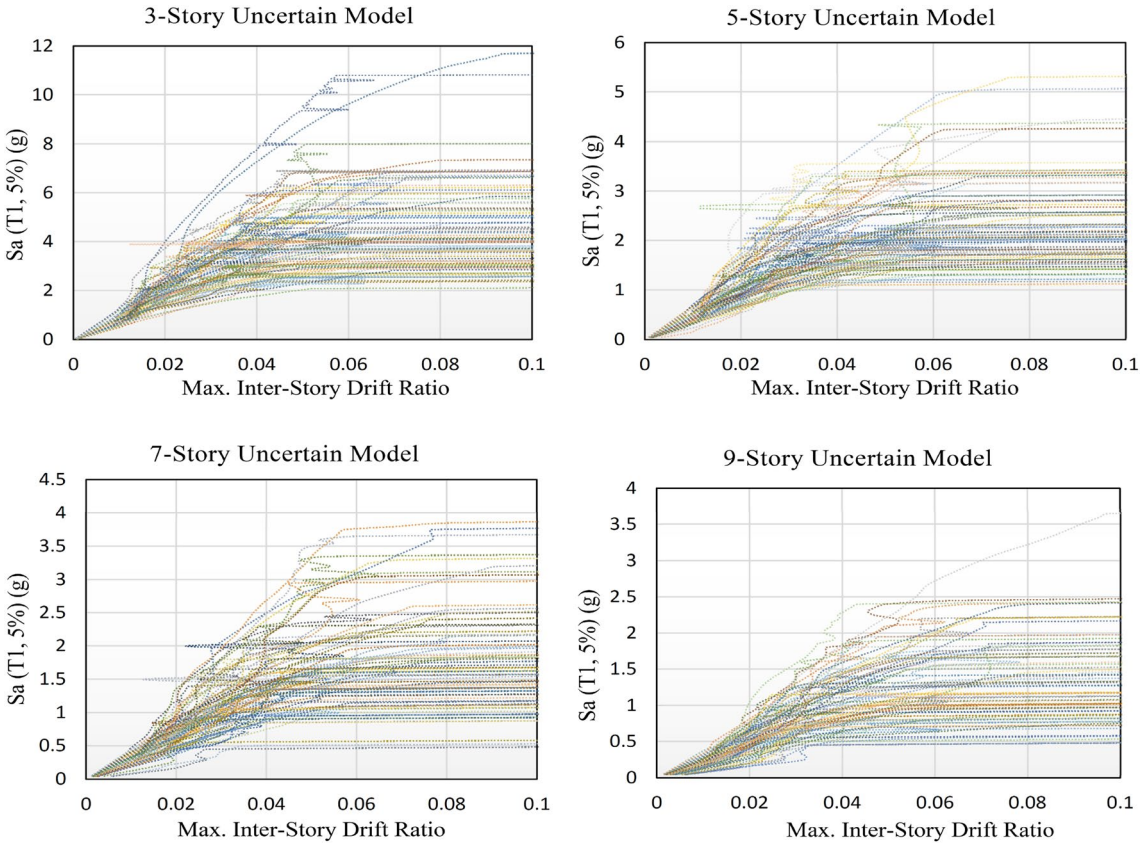

Fig. 6 IDA curves for 3–9 story frames (uncertain models)

where S_a represents the demand parameter in terms of intensity measure (IM), $S_{a,c}$ represents the limit state capacity presented in the form of spectral acceleration, v represents the seismicity rate and $f_{sa}(x)$ is the probability density function (PDF) for the defined IM and $H_{Sa}(x)$ denotes the seismic demand curve. The first term in the last equation is the fragility function of the spectral acceleration S_a. Accordingly, the λ_{LS} can be rewritten as follows:

$$\lambda_{LS=} \int F_{LS}(x).|dH_{S_a}(x)| \tag{9}$$

The latter equation shows how to extract λ_{LS} in terms of hazard and fragility functions. In other words, the above equation indicates that the mean annual frequency exceeding a given limit state (LS) is obtained by calculating the area under the graph of fragility function multiplied by the absolute value of the hazard derivative. According to the total probability theorem, the applied equation expresses λ_{LS} in the form of two separable functions of fragility and seismic hazard. The fragility function is calculated solely based on structural engineering analysis and the seismic hazard function is extracted from site seismological studies. This makes it possible to investigate the variations of λ_{LS} due to changes in the two functions mentioned above. Assuming fragility has lognormal distribution denoted by median μ and standard deviation σ and using Eq. (7) for the seismic hazard curve, the closed form of λ_{LS} can be expressed as follows (Jalayer & Cornell, 2004):

$$\lambda = k_0(\mu)^{-k}.e^{(\frac{1}{2}k^2.\beta^2)} \tag{10}$$

According to the above equation, to have a better understanding of the impact of capacity uncertainty on the estimation of MAF for the uncertain model (compared to the base model), the ratio of the mean annual frequency of the uncertain model to the base model ($\lambda_{cu}/\lambda_{cb}$) as a function of demand parameter (Maximum inter-story drift ratio) are shown in Figs. 13, 14.

By comparing the λ_c of the base and uncertain models, it can be seen that for average quality construction the capacity uncertainty has increased the MAF of the uncertain models at a collapse state of around 40% to 70%. This increase is due to the differences between the mean and standard deviation of the uncertain model's fragility function compared to the base model. In other words, in addition to increasing the standard deviation due to capacity uncertainty, a reduction

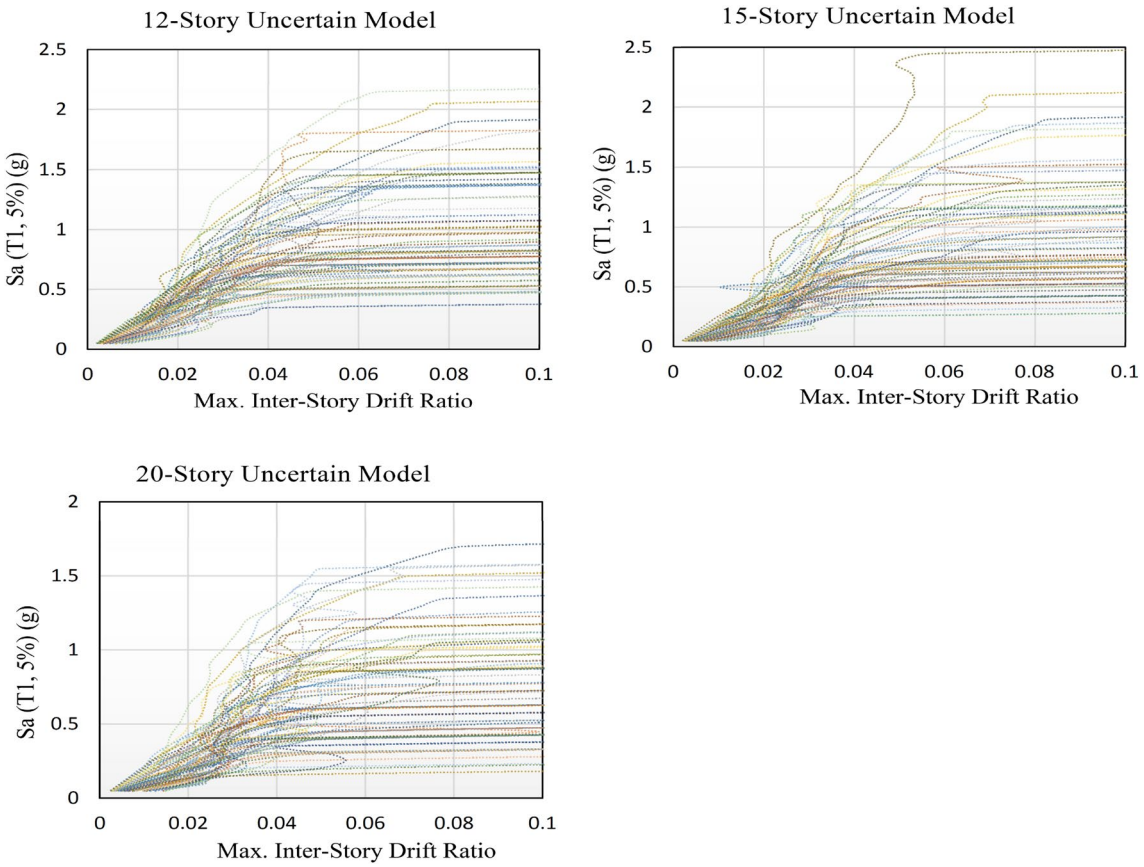

Fig. 7 IDA curves for 12–20 story frames (uncertain models)

in the median acceleration has a more pronounced effect to increase the mean annual frequency of the uncertain model.

It should be noted that despite the relatively small changes in the above values, there would be a meaningful increase in the mean annual frequency at the collapse state which has been less addressed in the previous studies (e.g. Vamvatsikos, 2014; Vamvatsikos & Fragiadakis, 2010)). In these studies, the investigation of capacity uncertainty was more focused on comparing the fragility curves. For this reason, despite confirming the reduction of the median spectral acceleration in the uncertain model, because of its less variation compared to the standard deviation, the base model median was considered acceptable for practical purposes and capacity uncertainty was considered only by increasing the standard deviation of the uncertain model compared to the base model (Vamvatsikos & Fragiadakis, 2010). Accordingly, comparing the base and uncertain models based on the fragility curves, which is a purely structural function, leads to an unrealistic underestimation of the global collapse probability of steel moment-resisting frames. Because, in this approach, the seismic hazard curve which is the occurrence probability of ground motion records used for extracting fragility curves is not taken into account. Based on the results, it is obvious that the impact of capacity uncertainty on deriving the mean annual frequency at the collapse state is not negligible.

To investigate the effect of each parameter of the fragility curve (median and standard deviation) on the estimation of the seismic demand assessment of steel moment-resisting frames, a sensitivity analysis based on the above-mentioned parameters is performed in the next section.

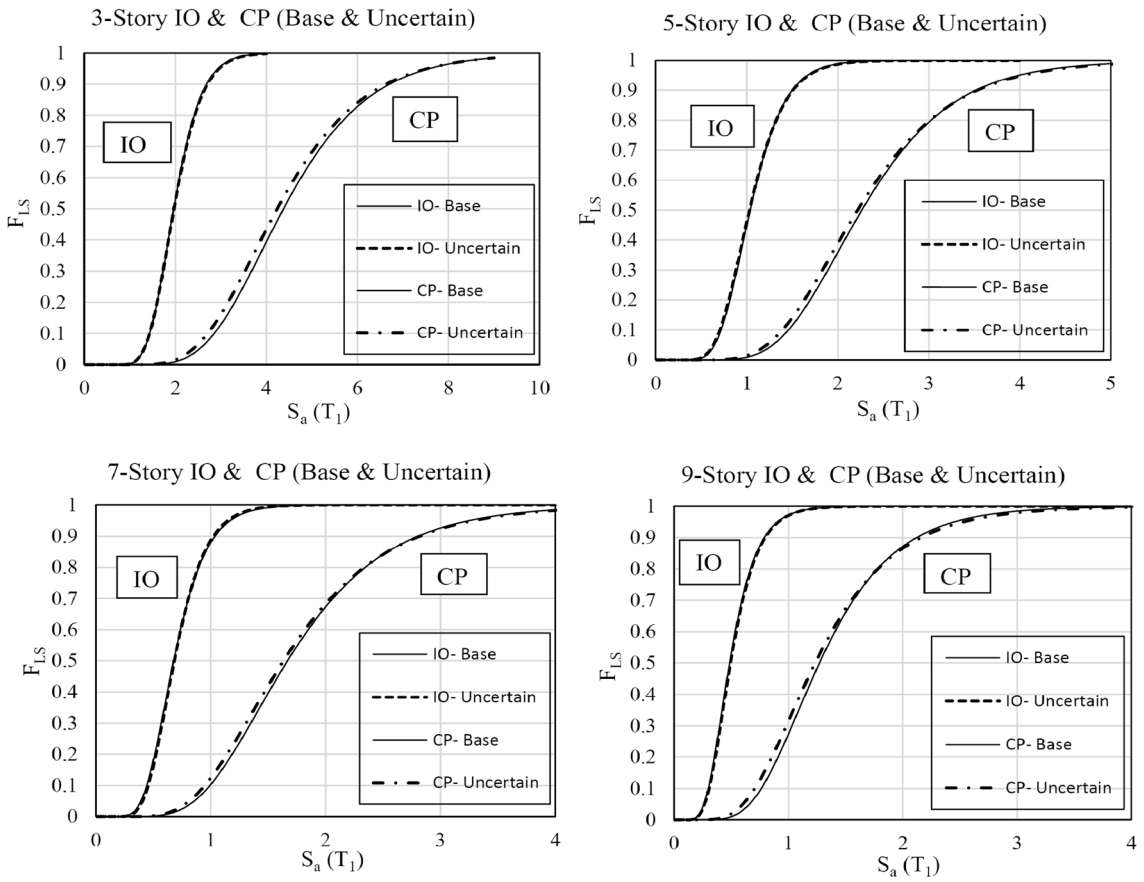

Fig. 8 3–9 story frames' fragility curves (base and uncertain)

Mean annual frequency sensitivity analysis

In the previous sections, the effect of capacity uncertainty on the seismic demand assessment of 7 steel moment frames was investigated and it was found that the model uncertainty increases significantly the mean annual frequency at the collapse state. Some of the factors causing capacity uncertainty are as follows:

- The precision of predicting experimental equations defining deterioration model parameters.
- Construction quality.

It was shown in the last section that estimating the probability of structural failure at the collapse limit state which is obtained by extracting the fragility function using the statistical lognormal distribution has enough acceptable accuracy to estimate that function. Hence it can be concluded that the effect of all uncertainties including the randomness of using different ground motion records and the epistemic capacity uncertainty leads to the derivation of the cumulative lognormal probability distribution for the fragility function. The properties of this function can be defined by two parameters, namely the mean and the standard deviation. The idea used in this study is to calculate the effect of capacity uncertainty on deriving λ_c in the form of sensitivity analysis of two dimensionless parameters of fragility curves: β_u/β_b and μ_b/μ_u. The first parameter is the standard deviation ratio of the uncertain model to the base model and the second parameter is the ratio of the base model median to the uncertain model.

To investigate the effect of the above-mentioned parameters on the ratio of the mean annual frequency of the uncertain model to the base model ($\lambda_{cu}/\lambda_{cb}$), the sensitivity analysis based on the variation of two defined parameters for the 20-story steel frame is performed.

According to Eq. 10, $\lambda_{cu}/\lambda_{cb}$ can be calculated as follows:

$$\frac{\lambda_{cu}}{\lambda_{cb}} = \left(\frac{\mu_b}{\mu_u}\right)^k .e^{\frac{1}{2}k^2.\beta_b^2\left[\left(\frac{\beta_u}{\beta_b}\right)^2-1\right]} \tag{11}$$

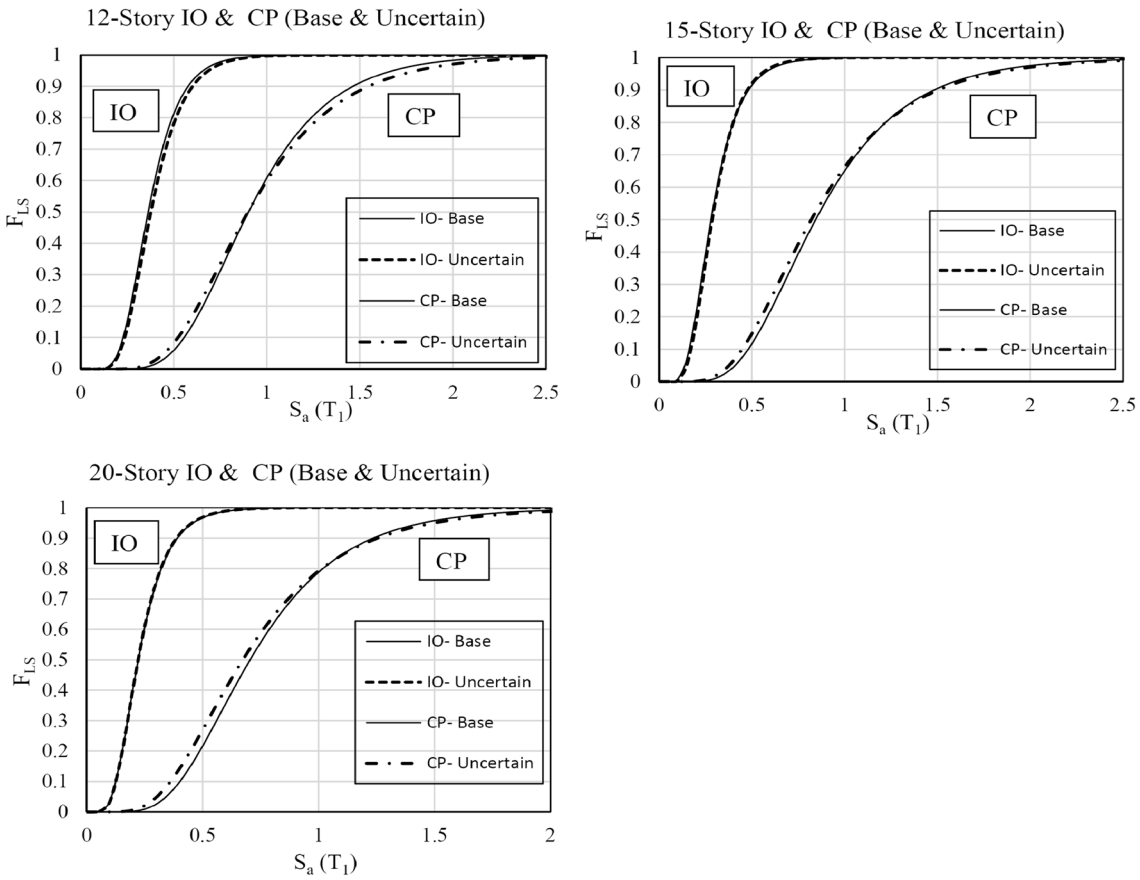

Fig. 9 12–20 story frames' fragility curves (base and uncertain)

Table 7 The base and the uncertain model (only due to model parameters) fragility function parameters

No. stories	Base model				Uncertain model			
	IO		CP		IO		CP	
	μ_{Sa}	$\sigma_{Ln\ Sa}$	μ_{Sa}	$\sigma_{Ln\ Sa}$	μ_{Sa}	$\sigma_{Ln\ Sa}$	μ_{Sa}	$\sigma_{Ln\ Sa}$
3	1.96	0.24	4.37	0.33	1.96	0.25	4.24	0.35
5	1.04	0.29	2.26	0.34	1.03	0.30	2.22	0.36
7	0.68	0.33	1.67	0.41	0.68	0.32	1.63	0.43
9	0.48	0.38	1.27	0.40	0.48	0.37	1.23	0.44
12	0.36	0.36	0.90	0.38	0.36	0.36	0.90	0.42
15	0.28	0.41	0.84	0.44	0.28	0.40	0.82	0.47
20	0.22	0.44	0.70	0.44	0.22	0.44	0.67	0.49

It can be seen from the above equation that the effect of the median change of the uncertain model on the variation of the $\lambda_{cu}/\lambda_{cb}$ ratio is only due to the k parameter of the seismic hazard curve (Eq. (7)) through a power relationship whereas the dispersion change of the uncertain model affects the $\lambda_{cu}/\lambda_{cb}$ ratio exponentially which depends on both the k factor of the hazard curve and the dispersion of the base model (β_b).

To have a better interpretation for the 20-story frame at the CP limit state ($k=2.7$ and $\beta_b=0.44$), two dimensionless parameters (β_u/β_b and μ_b/μ_u) are shown on the same horizontal axis and $\lambda_{cu}/\lambda_{cb}$ is shown on the vertical axis (Fig. 15). It can be seen that with a 30% increase in each of these two parameters, the mean annual frequency ratio increases by 63 and 103 percent, respectively. In addition, it is found that the impact of the median variation is more than the standard deviation variation. The reason is that according to

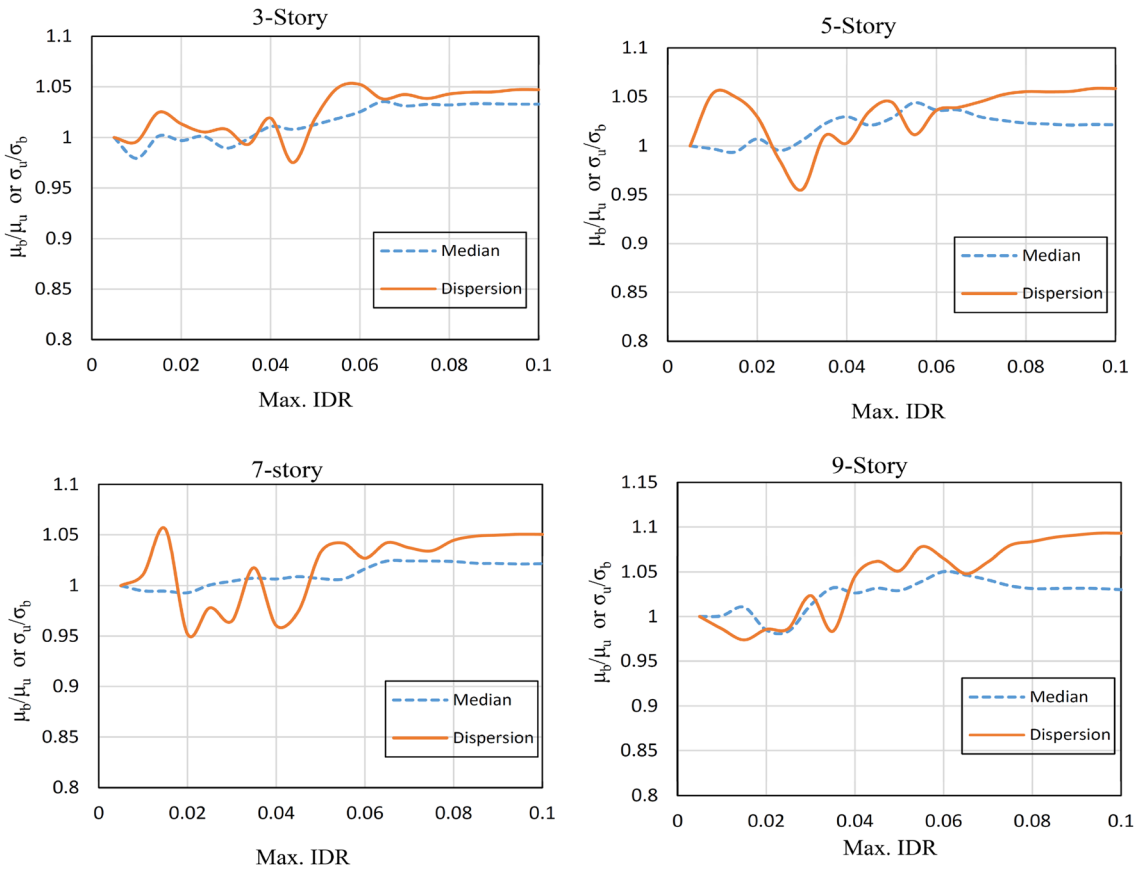

Fig. 10 3–9 story frames' median and dispersion ratio

Eq. (11) the slope of the median curve is more than the slope of the dispersion curve in high seismic-prone areas (Fig. 15). Accordingly, the adoption of the base model median for the uncertain model results in an underestimation of the MAF by about 13% for the 20-story frame.

Considering that the capacity uncertainty can change the median and dispersion together, the effect of simultaneous changes of two parameters is investigated in this section. For this purpose, the range of variations for each parameter is considered about 30% with 5% steps that cover an acceptable range of variations.

According to Eq. (11), the results of the bivariate sensitivity analysis for Century are shown in Table 9 and Fig. 16. It is clearly shown in Eq. (11) and Fig. 16 that the sensitivity of λ_c to median changes is somewhat higher than the dispersion variation. Therefore, if some factors cause more reduction of the uncertain model's median (e.g., bad construction quality), the mean annual frequency of the uncertain model will increase more severely.

It is noteworthy that due to the decomposition of the mean annual frequency in the form of the fragility and the seismic hazard curves, the applied methodology results in the derivation of the fragility curve in the form of a cumulative probability function that can be defined by two quantities (median and dispersion) and also the seismic hazard curve which can be represented by the attenuation equations on the other hand. The employed method can be readily applied to other structures such as reinforced concrete frames.

Conclusions

The seismic behavior of steel moment-resisting frames is always associated with some uncertainties. The considerable contribution of these uncertainties is due to the random nature of the ground motion record-to-record variability. Capacity uncertainty is another key factor that should be considered. In the present study, the impact of capacity uncertainty due to the model parameters and quality of construction on 7 steel moment-resisting frames (having similar building plans) is investigated. However, due to the way the model parameters are estimated which is based on experimental results and a limited number of samples, the application of these values will be associated with uncertainty. To apply this uncertainty, model parameters are perturbed by generating random numbers within the defined range of

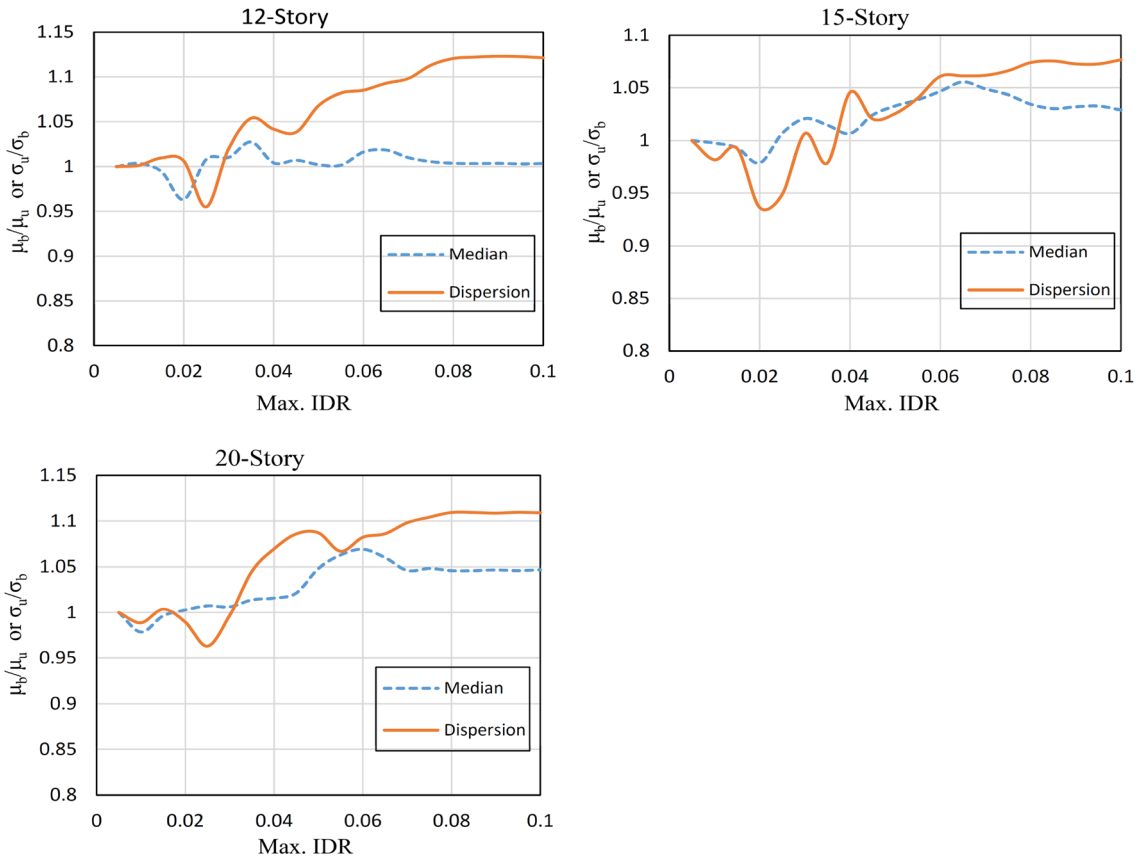

Fig. 11 12–20 story frames' median and dispersion ratio

Table 8 The base and the uncertain model fragility function parameters (average construction quality)

No. stories	Base model				Uncertain model			
	IO		CP		IO		CP	
	μ_{Sa}	$\sigma_{Ln\ Sa}$	μ_{Sa}	$\sigma_{Ln\ Sa}$	μ_{Sa}	$\sigma_{Ln\ Sa}$	μ_{Sa}	$\sigma_{Ln\ Sa}$
3	1.96	0.24	4.37	0.33	1.96	0.29	4.24	0.43
5	1.04	0.29	2.26	0.34	1.03	0.34	2.22	0.44
7	0.68	0.33	1.67	0.41	0.68	0.35	1.63	0.50
9	0.48	0.38	1.27	0.40	0.48	0.40	1.23	0.51
12	0.36	0.36	0.90	0.38	0.36	0.39	0.90	0.49
15	0.28	0.41	0.84	0.44	0.28	0.43	0.82	0.53
20	0.22	0.44	0.70	0.44	0.22	0.46	0.67	0.55

variation for each parameter and applied to the model. In addition, construction quality is considered by introducing additional dispersion according to the quality of frame building fabrication (superior-average-poor) (Fema, 2012). Fragility curves for the collapse limit state for both the base and the uncertain models are extracted. This is based on the results obtained from incremental dynamic analysis with 80 ground motion records and considering construction quality. In addition, MAF ratios are calculated for all frames based on capacity uncertainty at three levels of construction quality. In addition, a sensitivity analysis is performed on the MAF ratio in light of changes in the parameters of the fragility function. It can be concluded that ignoring the impact of capacity uncertainty results in a non-conservative estimation of the mean annual frequency (especially at the collapse state). However, it should be mentioned that the results of this study are limited to investigating 7 steel moment-resisting frames and further investigations are needed to more

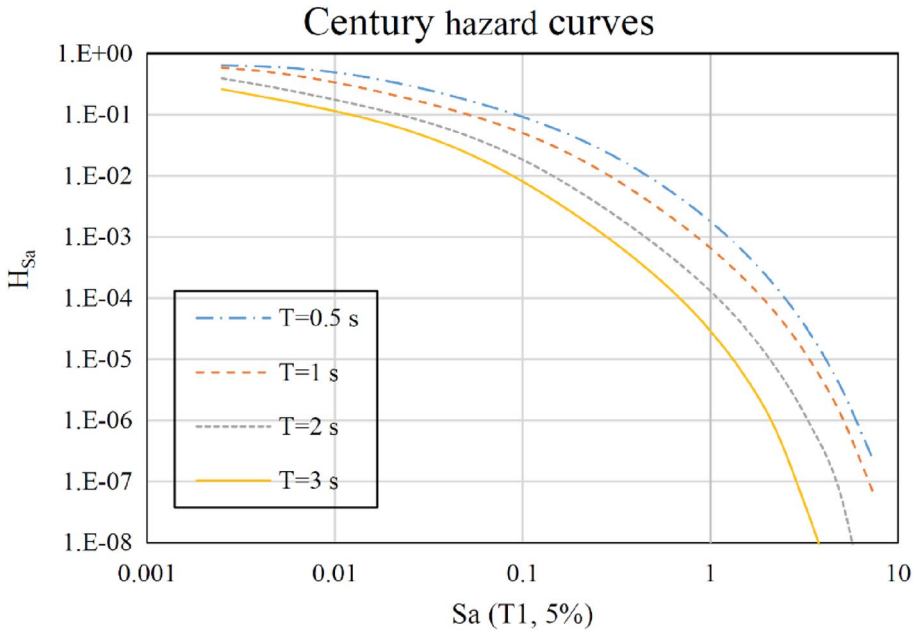

Fig. 12 The Century city hazard curves (Center, 2013)

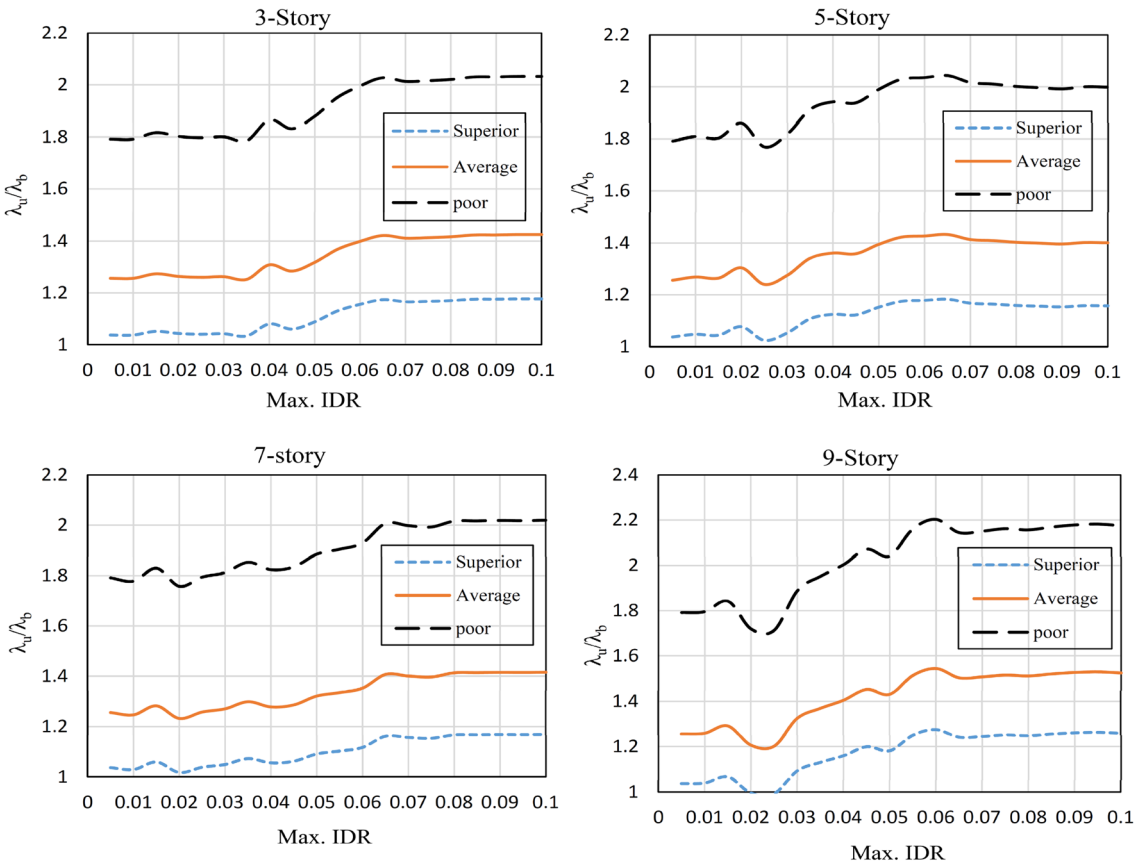

Fig. 13 3–9 story frames' MAF ratio

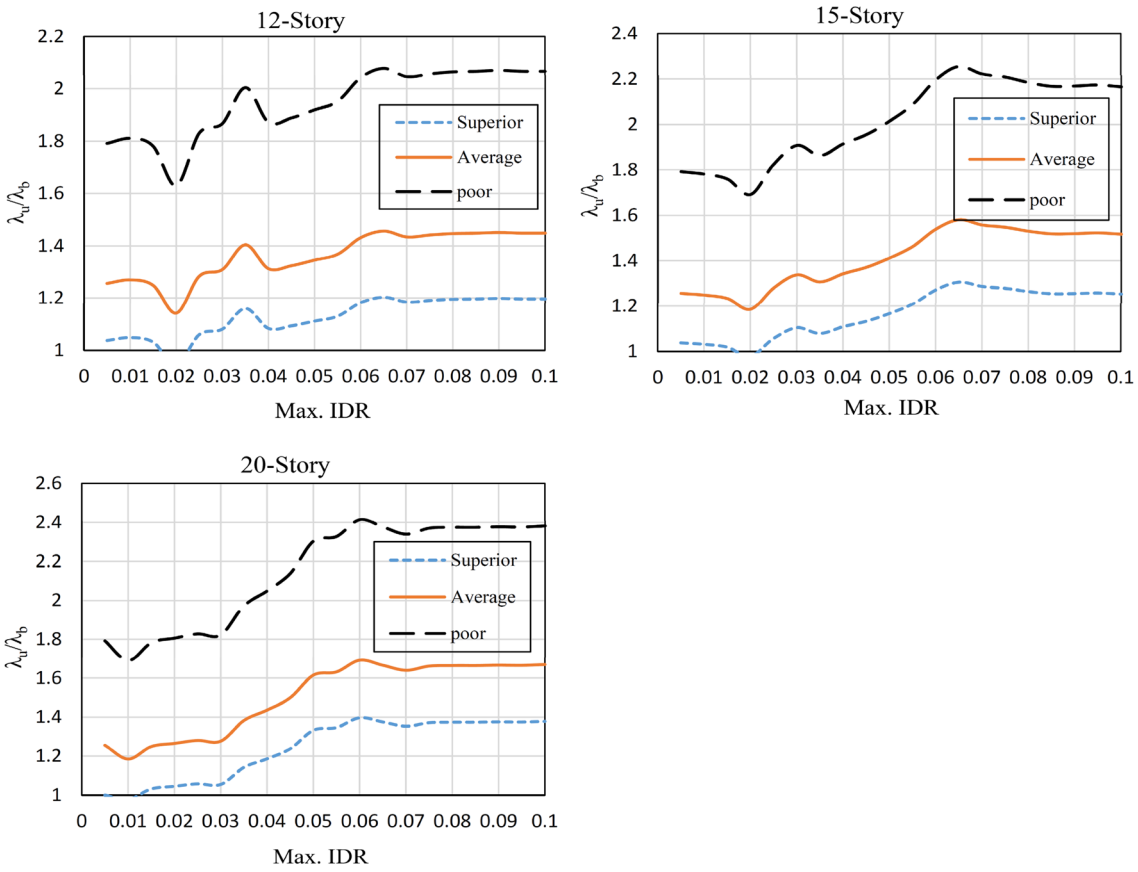

Fig. 14 12–20 story frames' MAF ratio

Fig. 15 λc sensitivity analysis based on independent changes of μ_b/μ_u and β_u/β_b

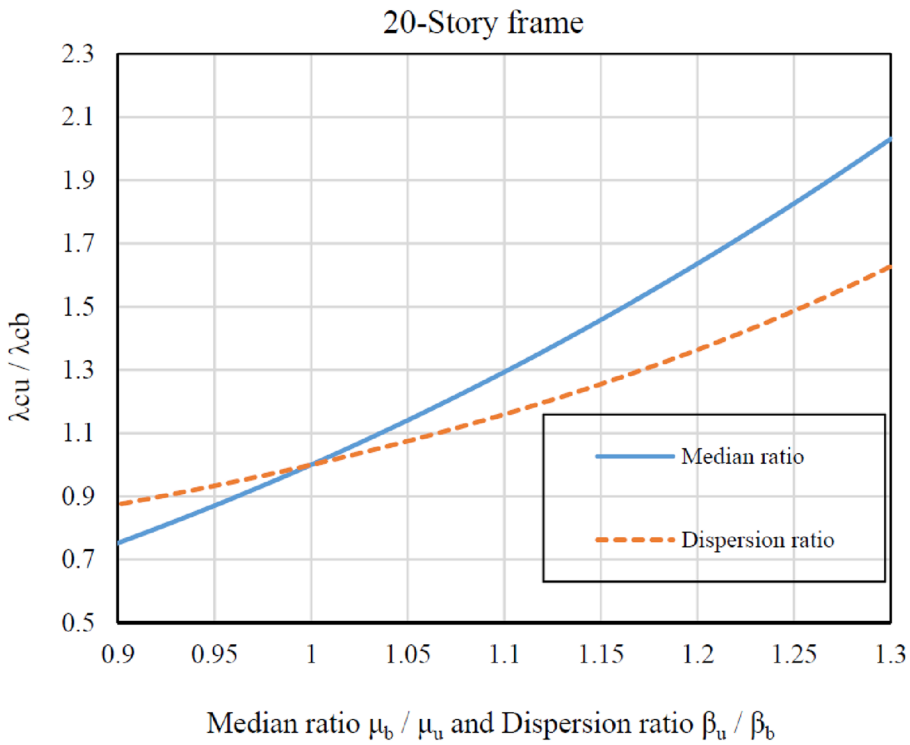

Table 9 λ_c sensitivity analysis based on the simultaneous changes of $\frac{\mu_b}{\mu_u}$ and $\frac{\beta_u}{\beta_b}$

$\lambda_{cu}/\lambda_{cb}$		β_u/β_b 1.00	β_u/β_b 1.05	β_u/β_b 1.1	β_u/β_b 1.15	β_u/β_b 1.2	β_u/β_b 1.25	β_u/β_b 1.3
μ_b/μ_u	1.00	1.000	1.075	1.160	1.256	1.364	1.487	1.627
μ_b/μ_u	1.05	1.141	1.226	1.323	1.432	1.556	1.697	1.856
μ_b/μ_u	1.10	1.293	1.391	1.500	1.624	1.764	1.924	2.105
μ_b/μ_u	1.15	1.458	1.568	1.691	1.831	1.989	2.169	2.373
μ_b/μ_u	1.20	1.636	1.759	1.897	2.054	2.232	2.433	2.662
μ_b/μ_u	1.25	1.827	1.964	2.118	2.293	2.492	2.717	2.972
μ_b/μ_u	1.30	2.031	2.183	2.355	2.550	2.770	3.020	3.305

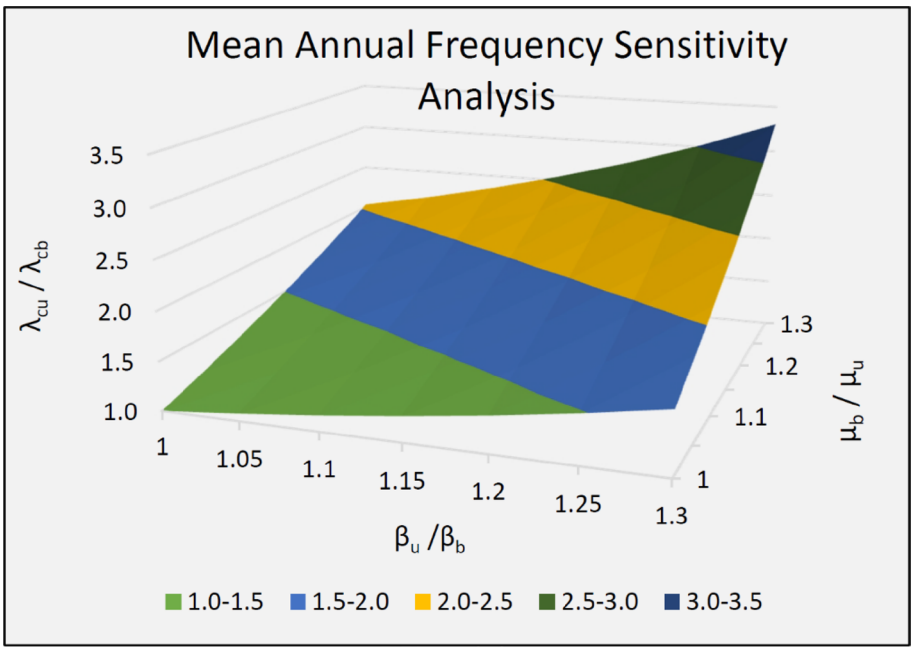

Fig. 16 λ_c sensitivity analysis graph

precisely evaluate the impact of capacity uncertainty on such frames. The major findings of the study can be summarized as follows:

1. Capacity uncertainty increases the dispersion and reduces the median of the fragility curves especially at the CP limit state. Compared to the base model, the variation of median and dispersion only caused by model parameters' uncertainty is about 4.5% and 11.4%, respectively. In addition, the classic idea of using the median of the base model for the uncertain model and applying capacity uncertainty through increasing dispersion can lead to underestimation of MAF for uncertain models.
2. As a result of capacity uncertainty, the MAF of uncertain models is higher than the MAF of base models. Thus, its effect on increasing the mean annual frequency is not negligible (particularly at demand parameter values exceeding 3 percent). Furthermore, if construction quality is taken into account, the MAF of the uncertain model will increase substantially. In comparison with base models, uncertain models have a higher MAF ratio of 20–40% for superior construction quality, 40–70% for average construction quality, and 120–140% for poor construction quality.
3. A sensitivity analysis of a 20-story frame indicates that median variation has a greater effect on increasing MAF ratio than standard deviation variation for uncertain models. This is because, according to Eq. (11), the slope of the median curve is higher than that of the dispersion curve in high seismic-prone areas. Also it can be used as a quick and efficient method to obtain a reasonable estimate of the MAF ratio for an uncertain model based on the results of the analysis for a base model.

Appendix

See Fig. 17 and Tables 10, 11, 12, 13, 14, 15, 16.

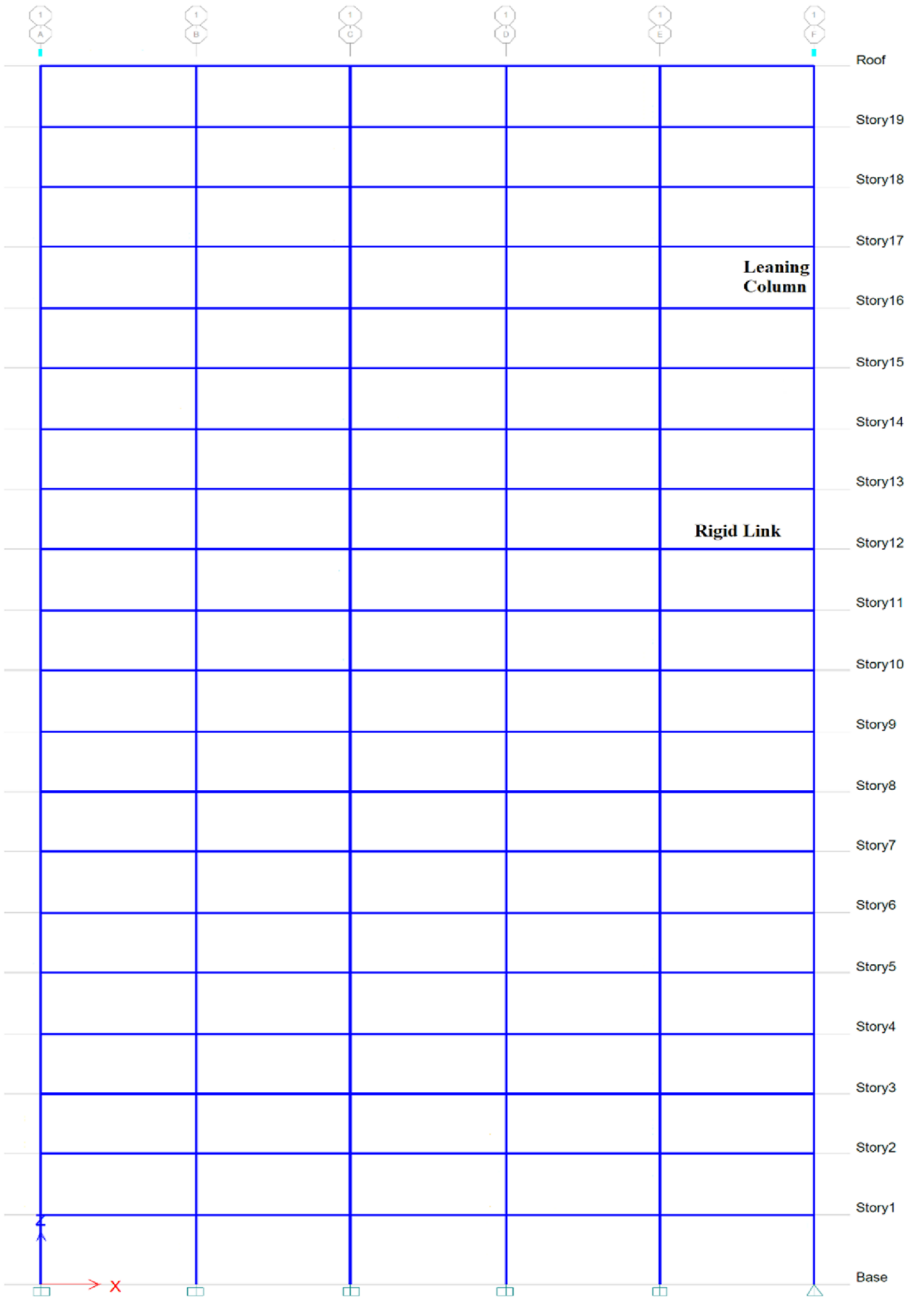

Fig. 17 20-story N–S Frame elevation (Mathiasson & Medina, 2014)

Table 10 N–S frame W-sections (20-story frame) (Mathiasson & Medina, 2014)

Floor	Story	Beams	Exterior columns	Interior columns
R	20	W24X94	W36X231	W36X231
20	19	W24X103	W36X231	W36X231
19	18	W30X148	W36X231	W36X231
18	17	W30X148	W36X231	W36X231
17	16	W36X182	W36X231	W36X247
16	15	W36X182	W36X231	W36X247
15	14	W36X194	W36X262	W36X302
14	13	W36X194	W36X262	W36X302
13	12	W36X232	W36X302	W36X330
12	11	W36X232	W36X302	W36X330
11	10	W36X256	W36X361	W36X395
10	9	W36X256	W36X361	W36X395
9	8	W36X256	W36X395	W36X395
8	7	W36X256	W36X395	W36X395
7	6	W36X262	W36X487	W36X441
6	5	W36X262	W36X487	W36X441
5	4	W36X282	W36X529	W36X487
4	3	W36X282	W36X529	W36X487
3	2	W36X282	W36X602	W36X487
2	1	W36X282	W36X602	W36X487

Table 11 N–S frame W-sections (15-story frame)

Floor	Story	Beams	Exterior columns	Interior columns
R	15	W24X94	W36X231	W36X231
15	14	W24X103	W36X231	W36X231
14	13	W30X148	W36X231	W36X247
13	12	W30X148	W36X231	W36X247
12	11	W36X148	W36X231	W36X302
11	10	W36X182	W36X231	W36X302
10	9	W36X182	W36X262	W36X330
9	8	W36X182	W36X262	W36X330
8	7	W36X194	W36X302	W36X395
7	6	W36X194	W36X302	W36X395
6	5	W36X194	W36X361	W36X395
5	4	W36X194	W36X361	W36X441
4	3	W36X194	W36X395	W36X441
3	2	W36X232	W36X395	W36X487
2	1	W36X232	W36X487	W36X487

Table 12 N–S frame W-sections (12-story frame)

Floor	Story	Beams	Exterior columns	Interior columns
R	12	W24X94	W36X231	W36X231
12	11	W24X103	W36X231	W36X231
11	10	W30X148	W36X231	W36X231
10	9	W30X148	W36X231	W36X247
9	8	W36X148	W36X231	W36X247
8	7	W36X148	W36X231	W36X302
7	6	W36X182	W36X262	W36X302
6	5	W36X182	W36X262	W36X330
5	4	W36X182	W36X302	W36X330
4	3	W36X182	W36X302	W36X330
3	2	W36X182	W36X361	W36X395
2	1	W36X182	W36X361	W36X395

Table 13 N–S frame W-sections (9-story frame)

Floor	Story	Beams	Exterior columns	Interior columns
R	9	W24X94	W36X231	W36X231
9	8	W24X103	W36X231	W36X231
8	7	W30X148	W36X231	W36X247
7	6	W30X148	W36X231	W36X247
6	5	W36X148	W36X231	W36X302
5	4	W36X148	W36X231	W36X302
4	3	W36X148	W36X262	W36X330
3	2	W36X182	W36X262	W36X330
2	1	W36X182	W36X302	W36X330

Table 14 N–S frame W-sections (7-story frame)

Floor	Story	Beams	Exterior columns	Interior columns
R	7	W24X94	W36X231	W36X231
7	6	W24X103	W36X231	W36X231
6	5	W30X148	W36X231	W36X231
5	4	W30X148	W36X231	W36X247
4	3	W30X148	W36X231	W36X247
3	2	W30X148	W36X231	W36X302
2	1	W36X182	W36X262	W36X302

Table 15 N–S frame W-sections (5-story frame)

Floor	Story	Beams	Exterior columns	Interior columns
R	5	W24X94	W36X231	W36X231
5	4	W24X103	W36X231	W36X231
4	3	W30X148	W36X231	W36X231
3	2	W30X148	W36X231	W36X231
2	1	W30X148	W36X231	W36X231

Table 16 N–S frame W-sections (3-story frame)

Floor	Story	Beams	Exterior columns	Interior columns
R	3	W24X94	W36X231	W36X231
3	2	W24X103	W36X231	W36X231
2	1	W30X148	W36X231	W36X231

Author contributions All authors contributed to the study conception and design. Material preparation, data collection and analysis were performed by BSY and MMA. The first draft of the manuscript was written by all authors and all authors commented on previous versions of the manuscript. All authors read and approved the final manuscript.

Funding The authors declare that no funds, grants, or other support were received during the preparation of this manuscript.

Data availability The authors declare that the data supporting the findings of this study are available within the paper.

Declarations

Conflict of interest The authors have no relevant financial or non-financial interests to disclose.

References

Adeli, M. M., Banazadeh, M., Deylami, A., & Alinia, M. (2012). Introducing a new spectral intensity measure parameter to estimate the seismic demand of steel moment-resisting frames using Bayesian statistics. *Advances in Structural Engineering, 15*(2), 231–247. https://doi.org/10.1260/1369-4332.15.2.231

Center, P. (2013). PEER ground motion database. *Pacific Earthquake Engineering Research Center, University of California, Berkeley, CA*. http://ngawest2.berkeley.edu.

Committee, A. (2010). *Minimum Design Loads for Buildings and Other Structures (ASCE/SEI 7–10)*. American Society of Civil Engineering, Reston, Virginia.

Cortés-Areizaga, G. (2007). Earthquake induced damage estimation for steel buildings in Puerto Rico (Doctoral dissertation, University of Puerto Rico, Mayaguez (Puerto Rico)).

Council, B. S. S. (2009). *NEHRP recommended seismic provisions for new buildings and other structures (FEMA P-750)*. Federal Emergency Management Agency.

FEMA, P., (2009). *Quantification of building seismic performance factors.*, *6*.

Fema, P. (2012). *58–1 (2012) Seismic performance assessment of buildings (volume 1-Methodology)*. Federal Emergency Management Agency.

Hamburger, R., Hooper, J., Sabol, T., Shaw, R., Reaveley, L., & Tide, R. (2000). *Recommended seismic design criteria for new steel moment-frame buildings (FEMA 350)*. In: Federal Emergency Management Agency.

Ibarra, L., & Krawinkler, H. (2011). Variance of collapse capacity of SDOF systems under earthquake excitations. *Earthquake Engineering & Structural Dynamics, 40*(12), 1299–1314. https://doi.org/10.1002/eqe.1089

Ibarra, L. F., Medina, R. A., & Krawinkler, H. (2005). Hysteretic models that incorporate strength and stiffness deterioration. *Earthquake Engineering & Structural Dynamics, 34*(12), 1489–1511. https://doi.org/10.1002/eqe.495

Jalayer, F., & Cornell, C. A. (2004). *A technical framework for probability-based demand and capacity factor design (DCFD) seismic formats*. Pacific Earthquake Engineering Research Center.

Kaveh, A., Azar, B. F., Hadidi, A., Sorochi, F. R., & Talatahari, S. (2010). Performance-based seismic design of steel frames using ant colony optimization. *Journal of Constructional Steel Research, 66*(4), 566–574. https://doi.org/10.1016/j.jcsr.2009.11.006

Kaveh, A., Fahimi-Farzam, M., & Kalateh-Ahani, M. (2015). Performance-based multi-objective optimal design of steel frame structures: Nonlinear dynamic procedure. *Scientia Iranica, 22*(2), 373–387.

Lignos, D., & Krawinkler, H. (2012). Sidesway collapse of deteriorating structural systems under seismic excitations. *Rep. No. TB 177, The John A. Blume Earthquake Engineering Research Center*. In: Stanford Univ., Stanford, CA.

Lignos, D. G., & Krawinkler, H. (2011). Deterioration modeling of steel components in support of collapse prediction of steel moment frames under earthquake loading. *Journal of Structural Engineering, 137*(11), 1291–1302.

Luco, N., & Cornell, C. A. (1998). *Seismic drift demands for two SMRF structures with brittle connections*. Structural Engineering World Wide.

Mathiasson, A., & Medina, R. A. (2014). Seismic collapse assessment of a 20-story steel moment-resisting frame structure. *Buildings, 4*(4), 806–822. https://doi.org/10.3390/buildings4040806

McKenna, F. (2011). OpenSees: A framework for earthquake engineering simulation. *Computing in Science & Engineering, 13*(4), 58–66. https://doi.org/10.1109/MCSE.2011.66

Medina, R. A., & Krawinkler, H. (2004). *Seismic demands for nondeteriorating frame structures and their dependence on ground motions*: Pacific Earthquake Engineering Research Center Berkeley.

Segura, C. L., Sattar, S., & Hariri-Ardebili, M. A. (2022). Quantifying material uncertainty in seismic evaluations of reinforced concrete bridge column structures. *ACI Structural Journal, 119*(3), 141–152. https://doi.org/10.14359/51734486

Sharma, V., Shrimali, M. K., Bharti, S. D., & Datta, T. K. (2020). Evaluation of responses of semi-rigid frames at target displacements predicted by the nonlinear static analysis. *Steel and Composite Structures, An International Journal, 36*(4), 399–415. https://doi.org/10.12989/scs.2020.36.4.399

Sharma, V., Shrimali, M., Bharti, S., & Datta, T. (2021). Seismic energy loss in semi-rigid steel frames under near-field earthquakes. In *Recent advances in computational mechanics and simulations* (pp. 431–443): Springer: Berlin.

Sharma, V., Shrimali, M. K., Bharti, S. D., & Datta, T. K. (2021). Seismic fragility evaluation of semi-rigid frames subjected to near-field earthquakes. *Journal of Constructional Steel Research, 176*, 106384. https://doi.org/10.1016/j.jcsr.2020.106384

Shinozuka, M. (1998). *Development of bridge fragility curves.* In Paper presented at the Proceedings of the US-Italy Workshop on Seismic Protective Systems for BridgesMultidisciplinary Center for Earthquake Engineering Research, Buffalo University, NY; Federal Highway Administration; the National Group for Defense Against Earthquakes of the Italian National Research Council.

Shome, N. (1999). *Probabilistic seismic demand analysis of nonlinear structures*. Stanford University.

Vamvatsikos, D. (2014). Seismic performance uncertainty estimation via IDA with progressive accelerogram-wise latin hypercube sampling. *Journal of Structural Engineering, 140*(8), A4014015. https://doi.org/10.1061/(ASCE)ST.1943-541X.0001030

Vamvatsikos, D., & Cornell, C. A. (2002). Incremental dynamic analysis. *Earthquake Engineering & Structural Dynamics, 31*(3), 491–514. https://doi.org/10.1002/eqe.141

Vamvatsikos, D., & Fragiadakis, M. (2010). Incremental dynamic analysis for estimating seismic performance sensitivity and uncertainty. *Earthquake Engineering & Structural Dynamics, 39*(2), 141–163.